ORIGINAL ARTICLES

Multimodal Imaging of Repetitive Transcranial Magnetic Stimulation Effect on Brain Network: A Combined Electroencephalogram and Functional Magnetic Resonance Imaging Study

Yafen Chen,[1] Yoon-Hee Cha,[2] Chuang Li,[3] Guofa Shou,[1]
Diamond Gleghorn,[2] Lei Ding,[1,3,4] and Han Yuan[1,3,4]

Abstract

Repetitive transcranial magnetic stimulation (rTMS) has been increasingly used to treat many neurological and neuropsychiatric disorders. However, the clinical response is heterogeneous mainly due to our inability to predict the effect of rTMS on the human brain. Our previous investigation based on functional magnetic resonance imaging (fMRI) suggested that neuroimaging-guided navigation for rTMS could be informed by understanding connectivity patterns that correlate with treatment response. In this study, 20 individuals with a balance disorder called Mal de Debarquement Syndrome completed high-density resting-state electroencephalogram (EEG) and fMRI recordings before and after 5 days of rTMS stimulation over both dorsolateral prefrontal cortices. Based on temporal independent component analysis of source-level EEG data, large-scale electrophysiological resting-state networks were reconstructed and connectivity values in each individual were quantified both before and after treatment. Our results show that high-density, resting-state EEG can reveal connectivity changes in brain networks after rTMS that correlate with symptom changes. The connectivity changes measured by EEG were primarily superficial cortical areas that correlate with previously shown default mode network changes revealed by fMRI. Further, higher baseline EEG connectivity values in the primary visual cortex were predictive of symptom reduction after rTMS. Our findings suggest that multimodal EEG and fMRI measures of brain networks can be biomarkers that correlate with the treatment effect of rTMS. Since EEG is compatible with rTMS, real-time navigation based on an EEG neuroimaging marker may augment rTMS optimization.

Keywords: brain stimulation; EEG; fMRI; functional connectivity; resting-state networks; Mal de Debarquement Syndrome

Introduction

MAL DE DEBARQUEMENT SYNDROME (MDDS) is a disorder of persistent oscillating vertigo caused by entrainment to background motion (Cha, 2009; Hain et al., 1999). This disorder is usually triggered by exposure to prolonged periods of low-frequency, low-amplitude oscillating motion such as sea or air travel. Brief periods of post motion feelings of rocking and swaying occur in the majority of individuals but are persistent for months or years in an important minority (Brown and Baloh, 1987). MdDS provides a non-injury brain

model of abnormal functional connectivity through which to study the effects of neuromodulation on motion perception.

Repetitive transcranial magnetic stimulation (rTMS) can induce lasting effects on human brain function (Hallett, 2007) and has gained broad acceptance in the treatment of neurological and psychiatric disorders; it has been experimentally investigated in the treatment of MdDS (Cha et al., 2016; Dell'Osso et al., 2009; Hasan et al., 2013). Our previous pilot studies of rTMS over the dorsolateral prefrontal cortex (DLPFC; Cha et al., 2013, 2016) showed that cortical stimulation could reduce symptoms of the oscillating vertigo of MdDS, even in

[1]Stephenson School of Biomedical Engineering, University of Oklahoma, Norman, Oklahoma.
[2]Laureate Institute for Brain Research, Tulsa, Oklahoma.
[3]School of Electrical and Computer Engineering, University of Oklahoma, Norman, Oklahoma.
[4]Institute for Biomedical Engineering, Science, and Technology, University of Oklahoma, Norman, Oklahoma.

medically refractory cases. The DLPFC was originally chosen as a target because prior imaging showed reduced glucose metabolism in the left prefrontal cortex as well as reduced prefrontal to limbic connectivity in individuals with MdDS (Cha et al., 2012). Our previous pilot studies of rTMS over DLPFC (Cha et al., 2013, 2016) showed that cortical stimulation could reduce symptoms of the oscillating vertigo of MdDS, even in medically refractory cases. The response to rTMS is heterogeneous, partially due to an incomplete understanding of the underlying mechanisms of rTMS and how such changes are related to therapeutic effects. However, measurement of functional neuroimaging changes related to symptom modification may help future protocol optimization.

Functional magnetic resonance imaging (fMRI) measures blood oxygen level-dependent signals and indirectly reflects human brain activity (Logothetis et al., 2001). Despite its limited temporal resolution on the level of seconds, fMRI has proven to be a useful neuroimaging modality in studying brain activation and brain synchrony between regional areas (Biswal et al., 1995). In contrast to fMRI, electroencephalogram (EEG) measures neuronal currents on a millisecond timescale with the ability to detect current sources at the cortical level by solving the so-called "inverse problem" (Grech et al., 2008). Nevertheless, in light of complementary features of EEG and fMRI, researchers have been able to combine those modalities (Mulert et al., 2004; Ritter and Villringer, 2006) to prospectively link the signals characterized by fMRI to phenomena revealed by EEG (Perry and Bentin, 2009; Yuan et al., 2016). This multimodal approach has been suggested to overcome the spatial resolution limitations of EEG and the temporal resolution limitations of fMRI. Further, it has the advantage of translating fMRI-based imaging to EEG-based imaging, which is portable and adaptable to versatile recording environments, such as those done simultaneously with rTMS (Ilmoniemi and Kičić, 2009).

Our previous investigation on fMRI revealed that a neuroimaging marker of resting-state functional connectivity (RSFC), particularly the connectivity between the entorhinal cortex (EC) and key nodes of the default mode network (DMN), was correlated with changes in perception of motion after rTMS in MdDS (Yuan et al., 2017). These findings suggested that a neuroimaging-based navigation strategy for determining rTMS targets might achieve a desirable pattern of connectivity after rTMS. Although fMRI may also provide connectivity feedback to inform the navigation of rTMS, it is not practical to obtain such information in an efficient manner. EEG, however, can be acquired interleaved with rTMS pulses, providing more rapid feedback on stimulation effects. Further, our recent study (Yuan et al., 2016) demonstrated an approach to reconstructing resting-state networks based on EEG data alone that resembles the spatiotemporal patterns of fMRI resting-state networks, suggesting that EEG-based connectivity markers may be promising surrogates of fMRI-based connectivity. Connectivity-informed targets could also improve therapeutic outcomes. Our current work aims at determining the correlation between fMRI imaging and EEG resting-state measurements, extending our prior work in studying EEG and fMRI connectivity measurements separately (Cha et al., 2018; Ding et al., 2014; Yuan et al., 2017). To determine symptom-related biomarkers, our study investigated pre- and post-TMS functional connectivity measurements on multimodal EEG and fMRI data that correlated with symptom status. We also examined baseline connectivity to determine whether any measures correlated with response to rTMS.

Materials and Methods

Participants

Study procedures were completed according to the Declaration of Helsinki guidelines and approved through the Western Institutional Review Board. Participants provided written informed consent and were recruited under ClinicalTrials.gov study NCT02470377. This study used rTMS in an off-label manner. Twenty individuals diagnosed with MdDS were included in this study. All participants provided written informed consent. The mean age of the participants was 52.9 ± 12.6 years, ranging from 28 to 76 years. The duration of illness had a mean of 35.2 ± 24.2 months, a median of 30 months, and a range of 8–96 months. All participants were female, which was consistent with the high prevalence of female sex in MdDS (Cha, 2009). Participants were included if they had: (1) persistent oscillating vertigo after disembarking from sea-, air-, and land-based travel that started within 2 days of disembarkation; (2) symptoms lasting at least 6 months; and (3) were evaluated by an experienced neurologist or otolaryngologist and were found to have no other cause for symptoms. In general, we recruited a medically refractory group that had failed vestibular therapy and at least two medication trials. Individuals were excluded if they: (1) had contraindications to undergoing rTMS or EEG/fMRI, such as medications known to reduce seizure threshold; (2) were pregnant or planned to be in the course of the study; (3) had an unclear trigger for their symptoms; (4) were incapable of completing all study-related testing; or (5) had an unstable medical or psychiatric condition such as a history of bipolar disorder or psychosis.

rTMS sessions

Both 1 Hz inhibitory and 10 Hz excitatory stimulation were administered to each participant at about the same time each day over five consecutive days (generally about 9 AM each day after registration for neuronavigation and calculation of motor thresholds [MTs]). The Localite TMS Navigator® frameless stereotaxy system was used to determine the center of the DLPFC as the location of the anterior portion of the middle frontal gyrus. rTMS was administered with the Magventure MagPro X100 stimulator with a cooled figure-of-eight coil in biphasic mode with the handle back at a 45° angle relative to the midsagittal plane. MTs for each motor hand cortex were determined each day for each participant. The hand knob landmark (Yousry et al., 1997) was identified by the neuronavigation system, and MTs were confirmed by evoking $50\,\mu V$ motor potential responses from the contralateral *abductor pollicis brevis* muscle. rTMS sessions were composed of 1 Hz stimulation over right DLPFC at 110% of right MT for 1200 pulses (20 min) and followed by 10 Hz stimulation over left DLPFC at 110% of left MT for 2000 pulses (25 min). The 10 Hz protocol was administered as a 26 sec rest after trains of 40 pulses over 4 sec.

Data acquisition

Both EEG and fMRI were performed on days 1 and 5 with rTMS sessions scheduled in the intervening days for each participant. Structural and resting-state fMRI were collected

by using a General Electric Discovery MR750 whole-body 3-Tesla magnetic resonance imaging (MRI) scanner (GE Healthcare, Milwaukee, WI). Whole-brain resting-state fMRI data were acquired by using the following parameters: field of view (FOV)/slice = 240/2.9 mm, axial slices per volume = 34, acquisition matrix = 96 × 96, repetition time/echo time (TR/TE) = 2000/30 ms, sensitivity encoding acceleration factor $R = 2$ in the phase encoding (anterior–posterior) direction, flip angle = 90°, and sampling bandwidth = 250 kHz. The echo-planar imaging images were reconstructed into a 128 × 128 matrix, in which the resulting fMRI voxel volume was $1.875 \times 1.875 \times 2.9$ mm^3. In addition, simultaneous physiological pulse oximetry and respiration waveform recordings were obtained (with 40 Hz sampling) for each fMRI run. A photo-plethysmograph with an infrared emitter placed under the pad of the subject's left index finger was used for pulse oximetry whereas a pneumatic respiration belt was used for respiration measurements. The subject rested quietly with their eyes closed during the image acquisitions. A T1-weighted magnetization-prepared rapid gradient-echo sequence with sensitivity encoding was used to provide an anatomical reference for the fMRI analysis, which had the following parameters: FOV = 240 mm, axial slices per slab = 190, slice thickness = 0.9 mm, image matrix = 256 × 256, TR/TE = 5/2.012 ms, acceleration factor $R = 2$, flip angle = 8°, inversion time TI = 725 ms, and sampling bandwidth = 31.2 kHz.

All EEGs were recorded through a 126-channel cap by using a BrainAmp amplifier (Brain Products GmbH, Munich, Germany). Sintered Ag/AgCl ring electrodes were mounted into the scalp cap according to the standard 10-5 system. Ten kiloohm was the impedance upper limit for all EEG electrodes. In the first 10 participants of the group, EEGs were acquired separately from fMRI at a sampling frequency of 1000 Hz while they were seated in a recliner and instructed to keep still with eyes closed during recording, which lasted 5 min (i.e., first cohort). In the second 10 participants, resting-state EEG was simultaneously obtained with fMRI at a sampling frequency of 5000 Hz for a period of 6 min and 10 sec (i.e., second cohort). Data from this second cohort were truncated to be 5 min to be consistent with the first cohort. The SyncBox device (Brain Products GmbH) was used to synchronize the internal sampling clock of the EEG amplifier with the MRI scanner 10 MHz master clock signal.

Visual analogue scale

A visual analogue scale (VAS) of 0–100 was employed to evaluate the participants' symptoms, in which 0 indicated a symptom-free state whereas 100 represented vertigo so severe that standing was not possible. The VAS reporting for each participant was done both before and after the five rTMS sessions and was used as a rapid state-based measurement. These data were part of a larger study that reported on longitudinal measurements with symptom-specific questionnaires (Cha et al., 2016). The differences between VAS scores both before and after rTMS were calculated, and participants were categorized as follows: Those whose scores decreased by 10 or more were considered to be ''positive responders,'' those whose score increased by 10 points or more were considered to be ''negative responders,'' and those whose scores changed between −10 and +10 were considered to be ''neutral respond-

ers.'' The threshold of 10 points was chosen because this is the level of difference on a 100 scale in which individuals with MdDS have a clear symptom change.

Resting-state fMRI analysis

fMRI data were preprocessed to remove any artifacts according to the pipeline described in Yuan et al. (2017). Specifically, the following steps were employed: respiration- and pulse-associated noise reduction, slice timing and rigid-body motion correction, spatial smoothing, temporal filtering with a bandpass filter (0.005–0.1 Hz), and regression for low-frequency changes in respiration volume, six affine motion parameters, signal from a ventricular region of interest (ROI), and signals from the white matter region. Data points with excessive motion were censored out in regression and correlation analyses.

Connectivity was calculated as the Pearson correlation between the seed region and the target regions. For further statistical analysis, Fisher transformation was employed to convert the correlation values into z-scores as the representation of RSFC. The seed region used was the left EC, which has been found to be hypermetabolic in MdDS in a previous functional imaging study with fluorodeoxyglucose positron emission tomography (PET; Cha et al., 2012). The coordinates of the individual EC locations were manually determined on high-solution structural magnetic resonance (MR) images acquired in the coronal plane by using anatomical guidelines by Insauti et al. (1998). To assess the cross-modal relationship, fMRI connectivity was compared with the connectivity of EEG networks. Specifically, the fMRI connectivity between the seed at the left EC and the inferior parietal lobule, the precuneus and the right EC were considered, since the modulation of RSFC at those regions was indicative of symptom changes after rTMS in our previous fMRI study (Yuan et al., 2017).

Resting-state EEG analysis

The pipeline of EEG analysis is shown in Figure 1. Data were cleaned of various environmental and physiological artifacts, including the MR gradient (only applied to MR-EEG), cardioballistic, muscle, and ocular movement-related artifact. Specifically, the gradient artifact and ECG artifact were removed in BrianVision Analyzer 2.1 based on average artifact subtraction (Allen et al., 2000). In addition, artifact residuals were removed through independent component analysis (ICA) in MATLAB 2016a. Bad channels with excessive artifacts were discarded via visual check (<1% on all data), with data from the discarded channels being replaced by an average of its nearby four channels. The percentage of bad epochs ranged from 0% to 0.191% and was not significantly different between pre- and post-TMS sessions (paired t-test, $p > 0.05$) or between response groups (analysis of variance, $p > 0.05$). High-pass filtering at 0.5 Hz and low-pass filtering at 70 Hz was applied. EEG raw data were downsampled to the microstate to retain data at a higher signal-to-noise ratio (Lehmann et al., 1987; Yuan et al., 2016). Boundary element models for all participants were built based on individual structural MRI data segmented by FreeSurfer (https://surfer.nmr.mgh.harvard.edu).

To run the group-level analysis, all individual head models underwent surface-based registration to the FreeSurfer ''fsaverage'' subject (Fischl et al., 1999). Individual digitization
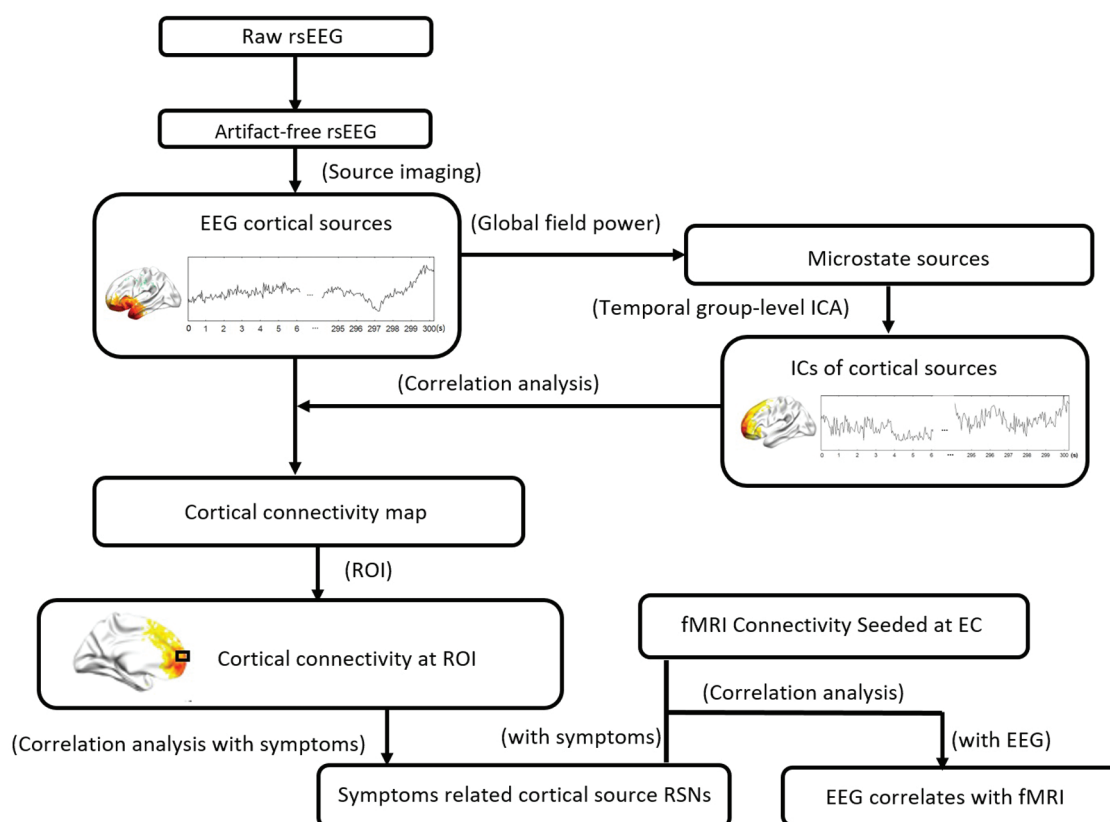
FIG. 1. EEG analysis pipeline. After preprocessing, rsEEG data were projected onto cortical surfaces through source imaging. Microstates on source signals were extracted, concatenated, and subject to group-level ICA performed. Cortical connectivity was calculated as the correlation between time courses of cortical sources and ICs. Connectivity values were extracted from ROIs and compared between pre- and post-TMS sessions with regard to symptom changes. EEG-based networks were also compared with the fMRI connectivity seeded at the EC. EC, entorhinal cortex; EEG, electroencephalogram; fMRI, functional magnetic resonance imaging; ICs, independent components; ICA, independent component analysis; ROIs, regions of interest; rsEEG, resting-state EEG; RSNs, resting state networks; TMS, transcranial magnetic stimulation. Color images are available online.

files of genuine electrode location were co-registered to the scalp model. EEG source imaging was used to back-project the sensor measurements on the scalp to the current dipoles on the cortex for each individual by a minimum norm method (Dale and Sereno, 1993; Hämäläinen and Ilmoniemi, 1994; see the following section for more details on source analysis). Absolute values of source data were temporally concatenated across participants and went through temporal ICA at a group level by using the infomax ICA algorithm implemented in the EEGLAB toolbox (http://sccn.ucsd.edu/eeglab). A total of 30 independent components (ICs) were calculated. The number of IC was chosen based on our previous investigation, which yielded cross-modal consistency between EEG and fMRI networks (Yuan et al., 2016). The EEG networks were compared with template fMRI networks derived from a large cohort of healthy individuals by Yeo et al. (2011), specifically the "Yeo 7 network" parcellation. Spatial correlation coefficients with Yeo template networks were calculated, and the IC with the highest spatial correlation was chosen as the match for a network. Six EEG networks were identified as significant matches to the corresponding template networks according to the null distribution of spatial correlation values established by a bootstrap approach in Yuan et al. (2016), including the DMN, the visual network,

the frontoparietal network, the motor network, the limbic network, and the dorsal attention network.

The EEG connectivity of each network was then calculated as the Pearson correlation between the time course of each temporal IC and the time courses of source dipoles on the cortical surface area for each subject. For statistical analyses, Pearson correlation coefficients on each map were converted to z-scores by Fisher's z transform. Pre- and post-TMS EEG connectivity maps were computed separately. The pre-TMS connectivity map is also referred to as the "baseline" connectivity map. "Post-minus-pre-connectivity" maps represent the connectivity changes after rTMS, which were calculated by subtracting the pre-TMS map from the post-TMS map for each participant.

Electrophysiological source imaging

For EEG source analyses, we used individual physical forward models linking the source dipoles to scalp EEG measurements. The forward model was constructed as a three-layer boundary element model composed of scalp, skull, and brain based on triangular elements. Each layer was given its own conductivity value (Zhang et al., 2006). Structural MRIs were implemented and employed to generate the

geometric models individually. Briefly, the forward model can be expressed in a linear equation as follows:

$$\Phi = A \cdot S + N, \tag{1}$$

where Φ is a matrix of the measured EEG, S is the unknown matrix of amplitudes of the source dipoles over time, A is the gain matrix, and N is a vector specifying the noise at each electrode.

There are a variety of linear inverse operators of the forward model. We used the minimum norm estimation method (Dale and Sereno, 1993; Hämäläinen and Ilmoniemi, 1994). The linear inverse operator for this method is expressed by:

$$W = RA^T (ARA^T + C)^{-1}, \tag{2}$$

where C and R are covariance matrices of the noise and sources, respectively.

Taken together, the minimum norm estimate of S, that is, S′ is computed as:

$$S' = W \cdot \Phi. \tag{3}$$

Associating EEG connectivity with symptom changes

The modulation on EEG networks was further examined with regard to symptom changes. We first defined ROIs based on the pre-TMS maps. Cortical surface area within a radius of 6 mm centered at the maximum of the IC map was drawn as an ROI (Sridharan et al., 2008). The ROIs' center coordinates are listed in Table 1. Connectivity values, that is, z-scores, within an ROI were extracted and averaged for each ROI. We then tested the relationship between EEG connectivity changes and symptom changes characterized by the VAS measurement. For example, a positive correlation coefficient signified a decrease in EEG connectivity related to a decrease of VAS scores. Similarly, if the connectivity increased when VAS scores increased, this would also be represented by a positive correlation coefficient. If connectivity increased while VAS decreased, or vice versa, the correlation coefficient would be negative. The method of controlling the false discovery rate by Benjamini and Yekutieli (2001) was employed for addressing the multiple comparison problem. The symbol q denotes the corrected p value. Further, to test whether the difference in connectivity was significant within each responder group, we performed paired, two-tailed t-tests on

TABLE 1. REGIONS OF INTEREST IN ELECTROENCEPHALOGRAM NETWORKS MATCHED TO TEMPLATES OF RESTING-STATE NETWORKS

Identified network	ROI	MNI coordinates (mm)		
		X	Y	Z
Default mode	lMFG	−20.26	57.80	1.819
Visual	lFG	28.42	−92.86	−12.55
Frontoparietal	rMFG	37.93	42.16	22.27
Motor	rPG	−57.80	−16.15	34.33
Limbic	rMTG	47.94	3.968	−33.87
Dorsal attention	lP	−8.610	−72.18	49.07

lFG, left Fusiform Gyrus; lMFG, left Medial Frontal Gyrus; lP, left Precuneus; MNI, the Montreal Neurological Institute; rMFG, right Middle Frontal Gyrus; rMTG, right Middle Temporal Gyrus; ROI, region of interest; rPG, right Precentral Gyrus.

the post-TMS and pre-TMS z-scores and the two-sample t-tests were employed for comparing connectivity between different groups. To test the normality of our data, we employed a corrected Kolmogorov–Smirnov test or LF KS test (Lilliefors, 1967; Öner and Deveci Kocakoç, 2017), with assumptions of unknown population mean and variance.

Associating EEG connectivity with fMRI

We investigated the relationship between EEG connectivity and fMRI-based connectivity. Since the EC has been identified as a region with metabolic and functional connectivity abnormalities in MdDS, we hypothesized that modulation by rTMS should change network connectivity to the EC. Unfortunately, surface-based EEG cannot measure electrical signals originating from the EC directly. Thus, instead of examining the direct effect on the EC, we investigated whether modulation of superficial cortical regions with functional connectivity with the EC could be affected, possibly through a cortical–subcortical pathway. We propose that changes in connectivity revealed in EEG networks are related to changes in fMRI connectivity to the EC. Thus, in our analyses, we compared the connectivity values of EEG networks in ROIs with the connectivity values of fMRI seeded within the EC. In particular, three cortical regions were considered based on our previous study (Yuan et al., 2017): the left precuneus, the right inferior parietal lobule, and the right EC. We computed the Pearson correlation between fMRI and EEG connectivity changes with these regions; regression lines were drawn to indicate the correlation between those two modalities.

EEG baseline connectivity prediction of treatment response

In addition to investigating symptom-related changes, we also examined whether baseline EEG connectivity is predictive of participants' responses after rTMS treatment. In this regard, we computed the cross-subject correlation between baseline connectivity and symptom changes indicated by VAS measurements. The prediction accuracy was tested for ROIs from EEG networks matched to the Yeo template.

Results

All 20 participants finished the rTMS protocol and imaging sessions. The symptom score changes from days 1 to 5 were evenly spread across the 20 participants. Six out of the 20 participants reported decreased symptoms after the treatment (VAS changes: −32.50 ± 17.56, "positive responders"), six of the participants felt slightly worse (VAS changes: +11.67 ± 3.73, "negative responders"), and the remaining eight participants reported unchanged symptoms (VAS changes: −1.38 ± 2.39 of VAS, "neutral responders"). For each cohort (first and second), the distribution of responses was identical: 30% positive, 30% negative, and 40% neutral. For both cohorts, the EEG sensor-level activity in individual topographies is illustrated in Supplementary Figure S1.

Since our previous PET and fMRI studies have indicated an important role of DMN in differentiating individuals with MdDS from the healthy controls (Cha et al., 2012) as well as being related to the symptom changes (Yuan et al., 2017), we first focused our investigation on the DMN. From EEG source data, one network was identified as the

match to the DMN of the Yeo template (Fig. 2A). Connectivity values within the ROI from the DMN were extracted from all individual pre- and post-rTMS images. Results revealed a significant correlation coefficient ($r = 0.54$, $q < 0.05$; Fig. 2C) between the difference in connectivity values and the changes in symptoms after rTMS. Specifically, a positive correlation indicated that greater symptom reduction was associated with a stronger decrease in connectivity within the DMN. The connectivity within the DMN in the positive subgroup was effectively reduced after TMS (paired t-test, $t(5) = -2.54$, $p = 0.05$; Fig. 2D). In comparison with the negative subgroup, the reduction of connectivity in the positive responders was significantly lower (unpaired t-test, $t(10) = -2.80$, $p = 0.02$; Fig. 2D).

We then extended our analysis to all the EEG networks identified in our procedure. A total of six networks matched the Yeo template networks (Yeo et al., 2011), that is, the visual, motor, dorsal attention, limbic, frontoparietal, and DMNs, with spatial correlations ranging from 0.21 to 0.45 (with mean ± standard deviation = 0.32 ± 0.091). Table 1 lists coordinates of the center of ROIs in all identified networks. The spatial patterns of all matched networks are illustrated in Supplementary Figure S2. Among the five EEG networks besides DMN, correlation analyses between ROI connectivity changes and VAS changes drew our attention to the visual network (Fig. 3A) and the limbic network (Fig. 4A). Similar to the DMN, modulations seen in the visual network across individuals were positively correlated with symptom changes ($r = 0.52$, $q < 0.05$; Fig. 3C). However, a reversed correlation was identified in the ROI of the limbic network, that is, the right middle temporal gyrus, in which a greater reduction of symptoms was associated with an increase in connectivity ($r = -0.61$, $q < 0.05$; Fig. 4C). In the subgroup of positive responders, the increase in EEG connectivity only approached significance ($t(5) = 2.45$, $p = 0.06$; Fig. 4D), yet it appeared to be higher than the changes in negative responders ($t(10) = 2.49$, $p = 0.03$; Fig. 4D).

To investigate the mechanism of rTMS modulation of EEG networks, we examined how EEG connectivity values are related to fMRI connectivity seeded at the EC. Our rationale was that although EEG cannot directly measure electrical activity originating from deep limbic structures, EEG is able to detect network connectivity of superficial cortical areas that co-modulate with those deep structures. Thus, we examined the cross-subject co-variation between the synchronization of EEG activities within a network (i.e., the
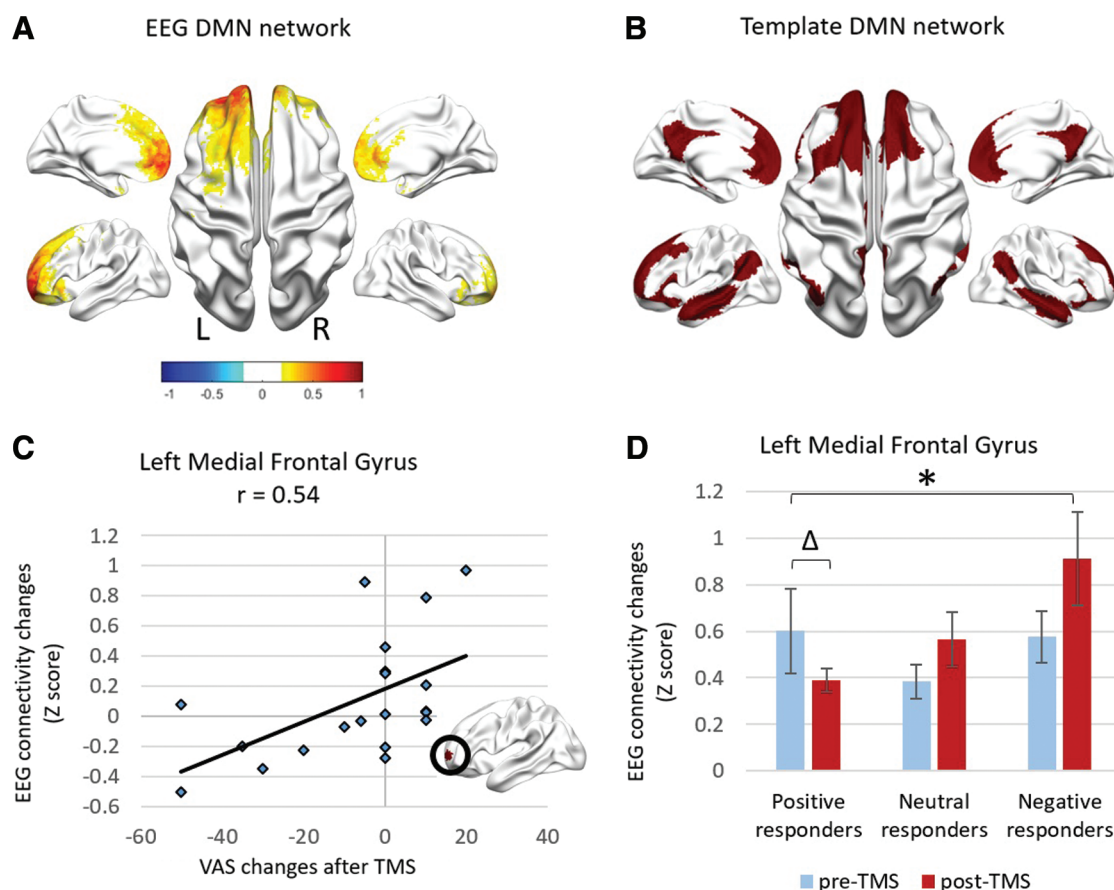

FIG. 2. Connectivity changes before and after rTMS in the DMN correlate with symptom changes. The DMN was identified in EEG **(A)**, which matched the fMRI template **(B)** by Yeo et al. (2011). The connectivity changes extracted from the ROI in the left medial frontal gyrus were positively correlated with symptom changes shown in **(C**; $q < 0.05$). Pre- and post-TMS values are shown in **(D)** for the subgroups of positive, neutral, and negative responders, separately. *Indicates significant between-group comparisons (positive responders vs. negative responders, unpaired t-test: $t(10) = -2.80$, $p = 0.02$). ^Δ^Indicates significant within-group comparison (paired t-test, $t(5) = -2.54$, $p = 0.05$). DMN, Default Mode Network; rTMS, repetitive transcranial magnetic stimulation; VAS, visual analogue scale. Color images are available online.
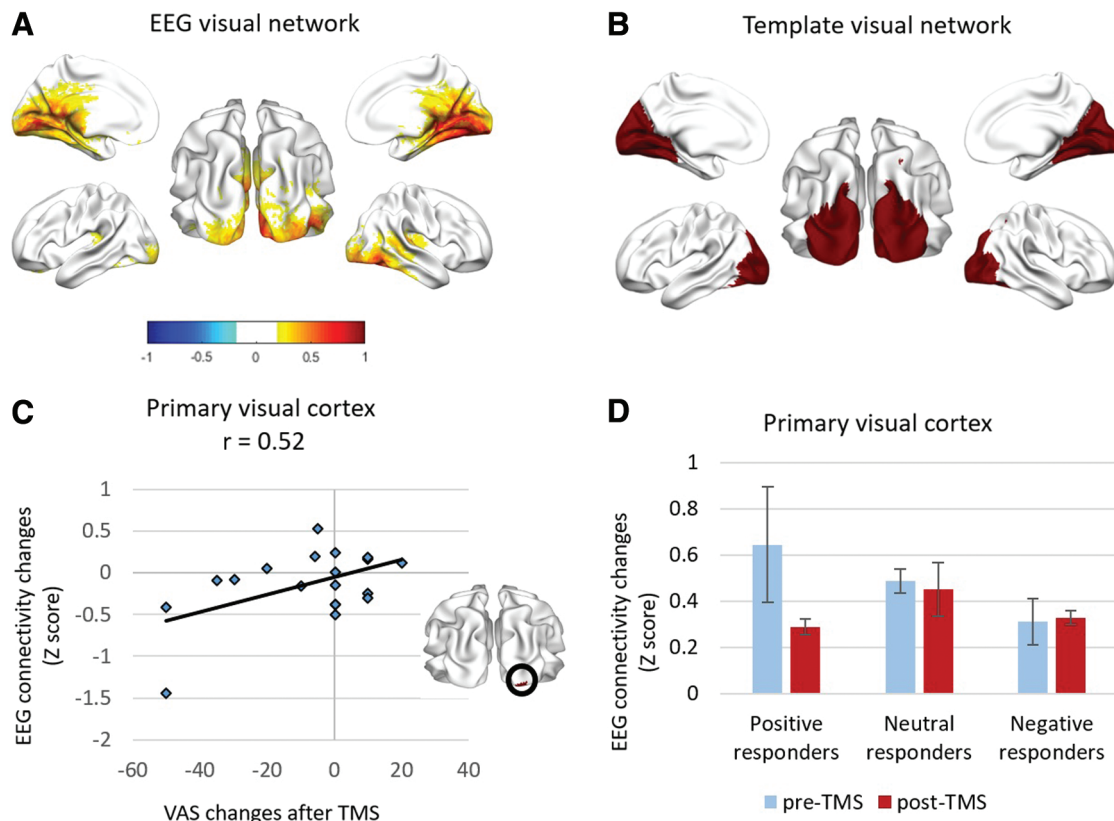
FIG. 3. Connectivity changes before and after rTMS in the visual network are correlated with symptom changes. A visual network was identified in EEG (**A**), which matched the fMRI template (**B**) by Yeo et al. (2011). The connectivity changes extracted from the ROI in the primary visual cortex were positively correlated with symptom changes as shown in (**C**; $q < 0.05$). Pre- and post-TMS values are shown in (**D**) for the subgroups of positive, neutral, and negative responders, separately. None of the between-group or within-group comparisons was significant. Color images are available online.

EEG network connectivity) and the synchronization of fMRI activities between two regions (i.e., the fMRI RSFC). As shown in Figure 5, the analysis revealed that EEG connectivity at the medial frontal gyrus within a DMN network co-varies with the RSFC between the EC and the right inferior parietal lobule ($r = 0.55$, $q < 0.05$).

Finally, we investigated whether the baseline EEG connectivity of several networks could be predictive of symptom changes after rTMS. As shown in Figure 6, baseline connectivity in the primary visual network was negatively correlated with symptom change ($r = -0.53$, $q < 0.05$), indicating that higher baseline connectivity predicted greater reduction of symptoms after rTMS. The baseline connectivity of the ROIs for the DMN and the limbic network are depicted in Supplementary Figures S3 and S4; the data did not reach significance. Nonetheless, in the left medial frontal gyrus, the majority of the participants' baseline connectivity followed a similar descending trend [i.e., higher baseline connectivity associated with greater symptom reduction ($r = -0.25$)], except one individual.

Discussion

Our study investigated the modulation effects of rTMS on brain networks by using multimodal neuroimaging data, that is, EEG and fMRI. In a group of MdDS participants, we were able to identify resting-state networks based on EEG data that

were matched to six fMRI template networks. The EEG network changes in the left medial frontal gyrus and primary visual cortex were positively correlated with symptom changes, whereas EEG network changes in the right middle temporal gyrus were negatively correlated with symptom changes. In addition, changes detected by EEG also correlated with fMRI-measured connectivity changes involving deeper cortical structures, particularly in a network that includes the EC and right inferior parietal lobule, all of which are nodes of the DMN. Further, baseline EEG connectivity values in the primary visual cortex were found to predict symptom changes induced by rTMS, with particularly high baseline connectivity predictive of reduction of symptoms.

The rTMS protocol employed in this study targeted both the left DLPFC and right DLPFC since our pilot studies of these two targets had previously demonstrated efficacy in relieving symptoms in some individuals with MdDS (Cha et al., 2013, 2016). Network analysis of EEG data revealed a significant correlation between modulations in connectivity and changes in symptoms. In particular, in the subgroup of positive responders to rTMS, reduction of symptoms was associated with a reduction of connectivity within the DMN. In the visual cortex, functional connectivity decreased after rTMS in 5 out of 6 positive responders. Notably, the visual cortex had been reported to possess higher connectivity with the EC in MdDS in a PET/fMRI study (Cha et al., 2012). This suggests that one of the therapeutic mechanisms

A EEG limbic network

B Template limbic network

C Right Middle Temporal Gyrus
r = -0.61
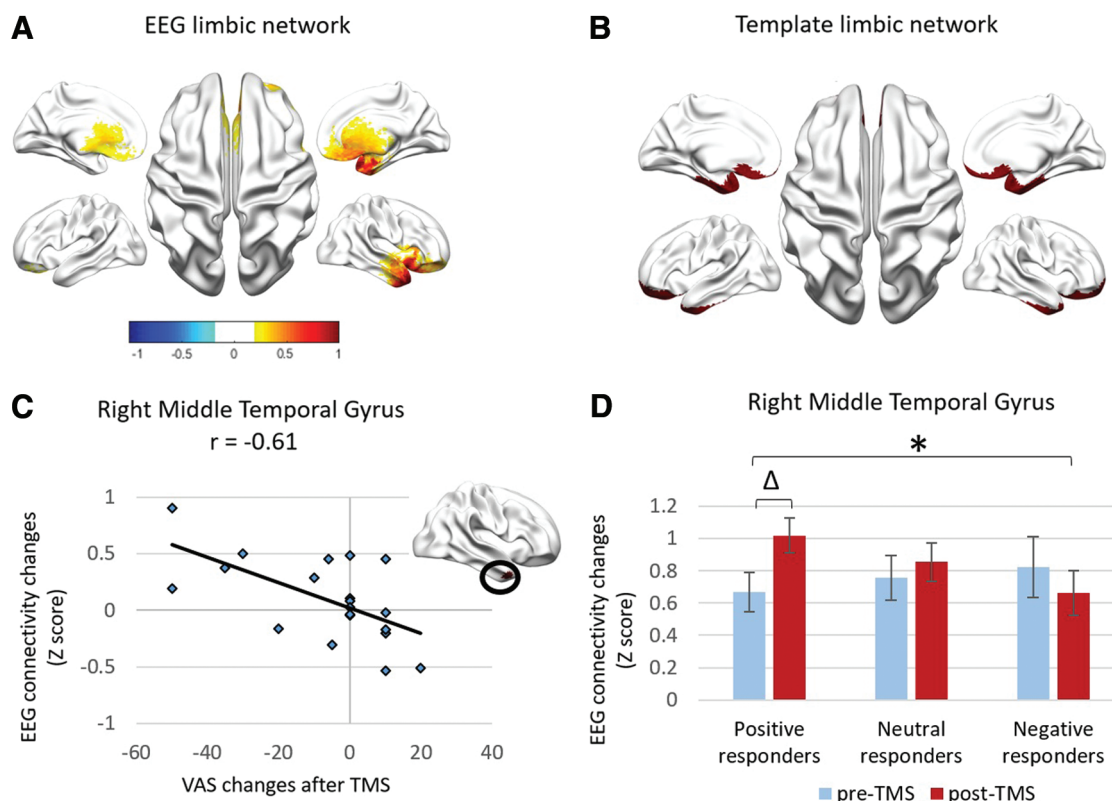
D Right Middle Temporal Gyrus

FIG. 4. Connectivity changes before and after rTMS in the limbic network are correlated with symptom changes. A limbic network was identified in EEG (**A**), which matched the fMRI template (**B**) by Yeo et al. (2011). The connectivity changes extracted from the ROI in the middle temporal gyrus were positively correlated with symptom changes as shown in (**C**; $q < 0.05$). Pre- and post-TMS values are shown in (**D**) for the subgroups of positive, neutral, and negative responders, separately. *Indicates significant between-group comparisons (positive responders vs. negative responders, unpaired t-test: $t(10) = 2.49$, $p = 0.03$). $^{\Delta}$Indicates within-group comparisons that approached significance (paired t-test, $t(5) = 2.45$, $p = 0.06$). Color images are available online.

of rTMS in MdDS may be to normalize hyperconnectivity in visual networks. In a prior investigation at the sensor level (Cha et al., 2018; Ding et al., 2014), a decrease of EEG connectivity was represented by a decrease in post-TMS neural synchrony over the posterior parietal and occipital areas.
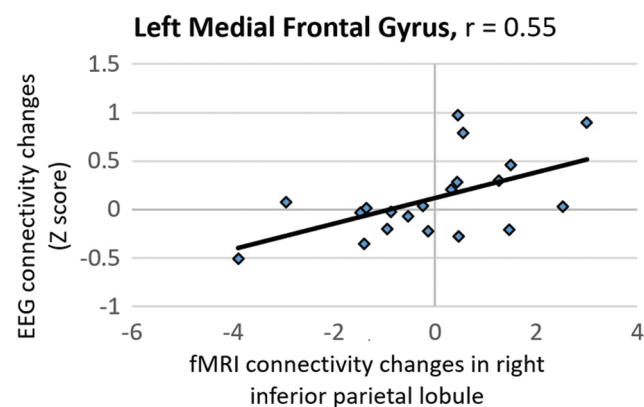
Left Medial Frontal Gyrus, r = 0.55

FIG. 5. Association between fMRI connectivity and EEG connectivity. Changes in fMRI connectivity between nodes of the DMN (i.e., the EC and inferior parietal lobule) are related to changes of the EEG network in the left medial frontal gyrus ($q < 0.05$). Color images are available online.

This decrease in synchrony was associated with an improvement in symptoms of MdDS, which are consistent with our findings in the source-level connectivity of visual cortex. In addition, this study has supported a role of the limbic network in MdDS. Such a network has been discovered in our previous investigation of EEG networks in healthy participants (the network E2 in Fig. 2 of Yuan et al., 2016). We observed a similar network in individuals with MdDS. Interestingly, our current results have revealed a reverse relationship between the modulation of limbic network connectivity and changes of symptoms, as compared with the DMN and visual networks. This region has not been broadly seen in our previous investigations (Cha et al., 2012; Ding et al., 2014), thus solid interpretation may warrant future study.

Other studies have investigated rTMS effects on brain networks such as in major depressive disorder (MDD). Liston et al. (2014) used 10-Hz rTMS targeting the left DLPFC in patients with depression and imaged them both before and after stimulation. They found that connectivity in the DMN was reduced significantly toward the lower connectivity level of healthy controls in treatment responders. Participants' symptom reductions were observed to be related to decreased connectivity within the DMN in another study by Philip et al. (2018), in which 5-Hz TMS was administered to the participants. Those results suggested that one mechanism of rTMS in alleviating depressive symptoms
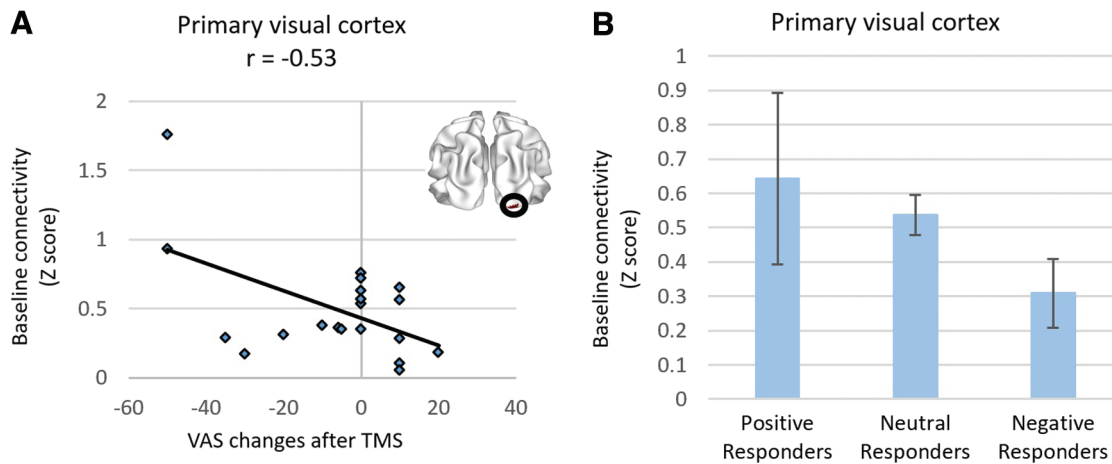
FIG. 6. Baseline connectivity in EEG visual network is related to symptom improvement. Pre-TMS connectivity extracted from the ROI in the primary visual cortex is correlated with symptom changes, as shown in **(A)**. The average connectivity values in the subgroups of the positive, neutral, and negative responders are shown in **(B)**. None of the between-group or within-group comparisons was significant. Color images are available online.

may be via normalization of the hyperconnectivity within the DMN. Considering that the left medial frontal gyrus is a key node within the DMN (Yeo et al., 2011), our observation of the positive correlation between DMN desynchronization and symptom improvement in MdDS emphasizes the important role of DMN in treating disorders of abnormal functional connectivity. In MdDS, desynchronization of visual cortex connectivity is also related to symptom improvement after rTMS implicating some disorder-specific effects that exist, in addition to more general signatures of maladaptive brain states.

Previous studies have revealed correspondence between fMRI and EEG resting-state networks in both temporal (Britz et al., 2010; Yuan et al., 2012) and spatial domains (Liu et al., 2017; Yuan et al., 2016), mainly in healthy subjects. In our study, symptom-related EEG synchronization changes over medial frontal gyrus complemented symptom-related RSFC changes shown by fMRI (Yuan et al., 2017). However, the locations where connectivity values were found to co-modulate in EEG and fMRI did not completely overlap, that is, EEG connectivity in medial frontal gyrus was shown to be related to RSFC in the inferior parietal cortex in fMRI. The reason may be different methodologies of identifying networks in EEG and fMRI: EEG networks were defined by using a data-driven approach, whereas fMRI connectivity was quantified with a seed-based approach. In addition, EEG networks capture connectivity among estimated electrophysiological sources whereas fMRI connectivity depicts pair-wise correlation in hemodynamics. Nonetheless, it is possible that a network-level interaction led to the relationship observed between connectivity in medial frontal gyrus and RSFC in inferior parietal cortex, which are all nodes of the DMN. Connectivity changes of both modalities showed consistent trends with symptom changes (i.e., positive relationship between two modalities in Fig. 5). Brain connectivity was mostly reduced in positive responders (Figs. 2C and 3C), a characteristic captured independently by both fMRI and EEG. This finding is consistent with the previous discovery of a close link between EEG and fMRI as indicators of brain activity across many brain regions (Goldman et al., 2002; Laufs et al., 2003; Yuan et al., 2016).

Further, our baseline analysis showed that, on average, higher pre-TMS connectivity over visual cortex (Fig. 6) predicted positive response. The connectivity between EC and motion processing areas such as the temporal and posterior occipital areas was found to be higher than in healthy controls (Cha et al., 2012). Those with higher baseline connectivity in visual areas may have had more room to change than those with lower connectivity. In a parallel fMRI study, Yuan et al. (2017) also reported that higher fMRI baseline connectivity between the rTMS targets (DLPFC) and EC (also a part of DMN) correlated with better treatment response. Higher RSFC was found to be critical in predicting positive treatment effects in other studies employing rTMS. In a study utilizing rTMS at DLPFC to treat patients with major depression, Liston et al. (2014) identified higher baseline RSFC in the positive response group compared with the poor response group. As a follow-up study, Avissar et al. (2017) reported that rTMS response could be predicted by higher RSFC in DLPFC-to-striatum in a larger subject study. Baeken et al. (2017) investigated theta burst stimulation effects on MDD subjects comparing their baseline connectivity with healthy controls, and they found that baseline RSFC between subgenual anterior cingulate and medial orbitofrontal cortex could distinguish responders from non-responders. Together, these findings support the prospect that measurements of RSFC before treatment could potentially be used to predict treatment responses in MdDS, MDD, and other disorders. This study shows that EEG can serve as a complementary modality in predicting treatment responses.

Our study suggests a strategy of using multimodal neuroimaging data to guide rTMS. These investigations have indicated that connectivity within the DMN, measured by fMRI as well as EEG, can be an imaging-based, objective symptom biomarker. Treatments guided by the modulation of this biomarker may be informative in trials of brain stimulation, potentially not limited to rTMS. More importantly, although fMRI is capable of revealing symptom-related connectivity, an EEG-based network is intriguing since it is compatible with rTMS and may provide instantaneous feedback in trials

of stimulation protocols. Further, biomarkers from the two modalities can be integrated to guide rTMS targets. For example, fMRI can be used to capture a disease-modifying network involving deep cortical or subcortical structures whereas connectivity involving superficial nodes of the network can be identified in EEG, potentially through a matching procedure with the fMRI-measured network as described in our study. Stimulation protocols could be adapted to promote networks modulation in desired directions. Many neurological disorders are characterized by dysfunction within the brain network rather than in isolated hubs or from structural injury (Fox et al., 2012). Integration of neuroimaging and neuromodulation protocols allows a broader platform of functional disorders to be investigated.

One limitation of this study is the lack of a sham condition to exclude non-specific effects of study participation. We had categorized the participants by symptom level at the time of image acquisition and contrasted responders and non-responders. The correlations were based on state-based measurements. Though a similar study could have been done by using the natural fluctuation of symptoms, this would have been impractical given the unpredictable nature of symptom changes. With rTMS, we were able to probe the neuroplasticity of the resting-state networks that are relevant to symptom level by creating a clearer separation of high versus low symptom states. A second limitation, partially related to creation of three response categories, is the low number of participants in each category. In our previous work, the "neutral" responders showed similar connectivity changes after TMS as the "negative" responders (Yuan et al., 2017). Perhaps owing to the greater magnitude in symptom change, "positive" responders (those who improved) showed connectivity changes that were distinct from either of the other two groups.

MdDS is a rare disorder that reveals the functional consequence of when the human brain encodes persistent periodic motion exposure. Until recently, there was no imaging correlate for this brain state. Our group has previously reported on both fMRI and EEG connectivity changes induced by rTMS; this study looks at the correlation between the two. Symptom fluctuations are typical in most neurological disorders but with a disorder such as MdDS, which is not related to any structural injury, alterations in functional connectivity itself could be the basis of symptom severity. Our study shows how EEG may be used as a complement to fMRI and perhaps as a replacement in cases in which high spatial resolution is not needed to more practically capture the neurological signatures of symptom changes.

Conclusion

This study employed a multimodal approach to examine the effect of rTMS treatment on brain networks in MdDS. Our findings demonstrated the feasibility of using EEG to characterize modulation of rTMS on brain networks that complements information from fMRI. Resting-state networks based on electrophysiological source images of EEG were reconstructed. The connectivity changes in the left medial frontal gyrus, the primary visual cortex, and the middle temporal gyrus correlated with symptom changes. More importantly, baseline connectivity values in the primary visual cortex emerged as a potential candidate that predicted symptom changes after rTMS, specifically with higher baseline connectivity being predictive of better treatment response.

Further, results of multimodal analyses indicate a mechanism of network-level modulation. The network modulation measured by EEG in superficial regions (i.e., medial frontal gyrus) was correlated to fMRI-based connectivity changes regarding the EC, implying that the observed modulation in superficial areas is due to coupling within the DMN. These findings suggest that network modulation can be an indicator of symptom changes to guide rTMS protocols. A multimodal approach leveraging the strengths of both EEG and fMRI at the network level may enhance the targeting of brain networks with rTMS and enhance clinical outcomes.

Author Disclosure Statement

No competing financial interests exist.

Supplementary Material

Supplementary Figure S1
Supplementary Figure S2
Supplementary Figure S3
Supplementary Figure S4

References

Allen PJ, Josephs O, Turner R. 2000. A method for removing imaging artifact from continuous EEG recorded during functional MRI. Neuroimage 12:230–239.

Avissar M, Powell F, Ilieva I, Respino M, Gunning FM, Liston C, Dubin MJ. 2017. Functional connectivity of the left DLPFC to striatum predicts treatment response of depression to TMS. Brain Stimul 10:919–925.

Baeken C, Duprat R, Wu GR, De Raedt R, van Heeringen K. 2017. Subgenual anterior cingulate-medial orbitofrontal functional connectivity in medication-resistant major depression: a neurobiological marker for accelerated intermittent theta burst stimulation treatment? Biol Psychiatry Cogn Neurosci Neuroimaging 2:556–565.

Benjamini Y, Yekutieli D. 2001. The control of the false discovery rate in multiple testing under dependency. Ann Statist 29: 1165–1188.

Biswal B, Yetkin FZ, Haughton VM, Hyde JS. 1995. Functional connectivity in the motor cortex of resting human brain using echo-planar MRI. Magn Reson Med 34:537–541.

Britz J, Van De Ville D, Michel CM. 2010. BOLD correlates of EEG topography reveal rapid resting-state network dynamics. Neuroimage 52:1162–1170.

Brown JJ, Baloh RW. 1987. Persistent Mal de Debarquement Syndrome: a motion-induced subjective disorder of balance. Am J Otolaryngol 8:219–222.

Cha YH. 2009. Mal de Debarquement. Semin Neurol 29:520–527.

Cha YH, Chakrapani S, Craig A, Baloh RW. 2012. Metabolic and functional connectivity changes in Mal de Debarquement Syndrome. PLoS One 7:e49560.

Cha YH, Cui YY, Baloh RW. 2013. Repetitive transcranial magnetic stimulation for Mal de Debarquement Syndrome. Otol Neurotol 34:175–179.

Cha YH, Shou G, Gleghorn D, Doudican BC, Yuan H, Ding L. 2018. Electrophysiological signatures of intrinsic functional connectivity related to rTMS treatment for Mal de Debarquement Syndrome. Brain Topogr 31:1047–1058.

Cha YH, Urbano D, Pariseau N. 2016. Randomized single blind sham controlled trial of adjunctive home-based tDCS after rTMS for Mal de Debarquement Syndrome: safety, efficacy, and participant satisfaction assessment. Brain Stimul 9:537–544.

Dale AM, Sereno MI. 1993. Improved localization of cortical activity by combining EEG and MEG with MRI cortical surface reconstruction—a linear-approach. J Cogn Neurosci 5:162–176.

Dell'Osso B, Mundo E, D'Urso N, Pozzoli S, Buoli M, Ciabatti M, et al. 2009. Augmentative repetitive navigated transcranial magnetic stimulation (rTMS) in drug-resistant bipolar depression. Bipolar Disord 11:76–81.

Ding L, Shou GF, Yuan H, Urbano D, Cha YH. 2014. Lasting modulation effects of rTMS on neural activity and connectivity as revealed by resting-state EEG. IEEE Trans Biomed Eng 61:2070–2080.

Fischl B, Sereno MI, Tootell RBH, Dale AM. 1999. High-resolution intersubject averaging and a coordinate system for the cortical surface. Hum Brain Mapp 8:272–284.

Fox MD, Halko MA, Eldaief MC, Pascual-Leone A. 2012. Measuring and manipulating brain connectivity with resting state functional connectivity magnetic resonance imaging (fcMRI) and transcranial magnetic stimulation (TMS). Neuroimage 62:2232–2243.

Goldman RI, Stern JM, Engel J, Jr., Cohen MS. 2002. Simultaneous EEG and fMRI of the alpha rhythm. Neuroreport 13:2487–2492.

Grech R, Cassar T, Muscat J, Camilleri KP, Fabri SG, Zervakis M, et al. 2008. Review on solving the inverse problem in EEG source analysis. J Neuroeng Rehabil 5:25.

Hain TC, Hanna PA, Rheinberger MA. 1999. Mal de Debarquement. Arch Otolaryngol Head Neck Surg 125:615–620.

Hallett M. 2007. Transcranial magnetic stimulation: a primer. Neuron 55:187–199.

Hämäläinen MS, Ilmoniemi RJ. 1994. Interpreting magnetic fields of the brain: minimum norm estimates. Med Biol Eng Comput 32:35–42.

Hasan A, Falkai P, Wobrock T. 2013. Transcranial brain stimulation in schizophrenia: Targeting cortical excitability, connectivity and plasticity. Curr Med Chem 20:405–413.

Insausti R, Juottonen K, Soininen H, Insausti AM, Partanen K, Vainio P, et al. 1998. MR volumetric analysis of the human entorhinal, perirhinal, and temporopolar cortices. Am J Neuroradiol 19:659–671.

Ilmoniemi RJ, Kičić D. 2009. Methodology for combined TMS and EEG. Brain Topogr 22:233.

Laufs H, Krakow K, Sterzer P, Eger E, Beyerle A, Salek-Haddadi A, Kleinschmidt A. 2003. Electroencephalographic signatures of attentional and cognitive default modes in spontaneous brain activity fluctuations at rest. Proc Natl Acad Sci U S A 100:11053–11058.

Lehmann D, Ozaki H, Pal I. 1987. EEG alpha map series: brain micro-states by space-oriented adaptive segmentation. Electroencephalogr Clin Neurophysiol 67:271–288.

Lilliefors HW. 1967. On the Kolmogorov-Smirnov test for normality with mean and variance unknown. J Am Stat Assoc 62:399–402.

Liston C, Chen AC, Zebley BD, Drysdale AT, Gordon R, Leuchter B, et al. 2014. Default mode network mechanisms of transcranial magnetic stimulation in depression. Biol Psychiatry 76:517–526.

Liu Q, Farahibozorg S, Porcaro C, Wenderoth N, Mantini D. 2017. Detecting large-scale networks in the human brain using high-density electroencephalography. Hum Brain Mapp 38:4631–4643.

Logothetis NK, Pauls J, Augath M, Trinath T, Oeltermann A. 2001. Neurophysiological investigation of the basis of the fMRI signal. Nature 412:150.

Mulert C, Jager L, Schmitt R, Bussfeld P, Pogarell O, Moller HJ, et al. 2004. Integration of fMRI and simultaneous EEG: towards a comprehensive understanding of localization and time-course of brain activity in target detection. Neuroimage 22:83–94.

Öner M, Deveci Kocakoç İ. 2017. JMASM 49: a compilation of some popular goodness of fit tests for normal distribution: their algorithms and MATLAB codes (MATLAB). J Mod Appl Stat Methods 16:30.

Perry A, Bentin S. 2009. Mirror activity in the human brain while observing hand movements: a comparison between EEG desynchronization in the mu-range and previous fMRI results. Brain Res 1282:126–132.

Philip NS, Barredo J, van't Wout-Frank M, Tyrka AR, Price LH, Carpenter LL. 2018. Network mechanisms of clinical response to transcranial magnetic stimulation in posttraumatic stress disorder and major depressive disorder. Biol Psychiatry 83:263–272.

Ritter P, Villringer A. 2006. Simultaneous EEG–fMRI. Neurosci Biobehav Rev 30:823–838.

Sridharan D, Levitin DJ, Menon V. 2008. A critical role for the right fronto-insular cortex in switching between central-executive and default-mode networks. Proc Natl Acad Sci U S A 105:12569–12574.

Yeo BT, Krienen FM, Sepulcre J, Sabuncu MR, Lashkari D, Hollinshead M, et al. 2011. The organization of the human cerebral cortex estimated by intrinsic functional connectivity. J Neurophysiol 106:1125–1165.

Yousry TA, Schmid UD, Alkadhi H, Schmidt D, Peraud A, Buettner A, Winkler P. 1997. Localization of the motor hand area to a knob on the precentral gyrus. A new landmark. Brain 120(Pt. 1):141–157.

Yuan H, Ding L, Zhu M, Zotev V, Phillips R, Bodurka J. 2016. Reconstructing large-scale brain resting-state networks from high-resolution EEG: spatial and temporal comparisons with fMRI. Brain Connect 6:122–135.

Yuan H, Shou G, Gleghorn D, Ding L, Cha YH. 2017. Resting state functional connectivity signature of treatment effects of repetitive transcranial magnetic stimulation in Mal de Debarquement Syndrome. Brain Connect 7:617–626.

Yuan H, Zotev V, Phillips R, Drevets WC, Bodurka J. 2012. Spatiotemporal dynamics of the brain at rest—exploring EEG microstates as electrophysiological signatures of BOLD resting state networks. Neuroimage 60:2062–2072.

Zhang Y, van Drongelen W, He B. 2006. Estimation of *in vivo* brain-to-skull conductivity ratio in humans. Appl Phys Lett 89:223903–2239033.

Address correspondence to:
Han Yuan
Stephenson School of Biomedical Engineering
University of Oklahoma
202 W. Boyd Street, Room 107
Norman, OK 73019

E-mail: hanyuan@ou.edu